Phosphoryl Transfer Is Not Rate-Limiting for the ROCK I-Catalyzed Kinase Reaction

Olga Futer, Ahmad R. Saadat, John D. Doran, Scott A. Raybuck, and S. Pazhanisamy*

Vertex Pharmaceuticals Incorporated, 130 Waverly Street, Cambridge, Massachusetts 02139-4242

Received December 2, 2005; Revised Manuscript Received April 27, 2006

ABSTRACT: Rho-associated coiled−coil kinase, ROCK, is implicated in Rho-mediated cell adhesion and smooth muscle contraction. Animal models suggest that the inhibition of ROCK can ameliorate conditions, such as vasospasm, hypertension, and inflammation. As part of our effort to design novel inhibitors of ROCK, we investigated the kinetic mechanism of ROCK I. Steady-state bisubstrate kinetics, inhibition kinetics, isotope partition analysis, viscosity effects, and presteady-state kinetics were used to explore the kinetic mechanism. Plots of reciprocals of initial rates obtained in the presence of nonhydrolyzable ATP analogues and the small molecule inhibitor of ROCK, Y-27632, against the reciprocals of the peptide concentrations yielded parallel lines (uncompetitive pattern). This pattern is indicative of an ordered binding mechanism, with the peptide adding first. The staurosporine analogue K252a, however, gave a noncompetitive pattern. When a pulse of ^{33}P-γ-ATP mixed with ROCK was chased with excess unlabeled ATP and peptide, 0.66 enzyme equivalent of ^{33}P-phosphate was incorporated into the product in the first turnover. The presence of ATPase activity coupled with the isotope partition data is a clear evidence for the existence of a viable [E−ATP] complex in the kinase reaction and implicates a random binding mechanism. The k_{cat}/K_m parameters were fully sensitive to viscosity (viscosity effects of 1.4 ± 0.2 and 0.9 ± 0.3 for ATP and peptide **5**, respectively), and therefore, the barriers to dissociation of either substrate are higher than the barrier for the phosphoryl transfer step. As a consequence, not all the binding steps are at fast equilibrium. The observation of a burst in presteady-state kinetics ($k_b = 10.2 \pm 2.1$ s^{-1}) and the viscosity effect on k_{cat} of 1.3 ± 0.2 characterize the phosphoryl transfer step to be fast and the release of product and/or the enzyme isomerization step accompanying it as rate-limiting at V_{max} conditions. From the multiple kinetic studies, most of the rate constants for the individual steps were either evaluated or estimated.

Binding agonists such as 5-HT[1], angiotensin II, and PDGF to receptors at the cell surface relay specific signals inside the cell. Small GTPases of the Rho family are one of the primary mediators of the signals from such extracellular stimuli. Rho GTPases play a central role in Ca^{2+}-sensitized vascular smooth muscle contraction (*1*), actin cytoskeleton reorganization (*2*), negative regulation of neurite growth (*3*), cell migration (*4*), adhesion and motility (*5*), and cytokinesis (*6*). Modulating the Rho-mediated signaling is, therefore, potentially beneficial for treating hypertension (*7*−*8*), atherosclerosis (*9*), cancer (*10*), inflammation (*11*), fibrosis (*12*), and vasospasm (*13*). The various activities of Rho appear to be regulated by multiple signaling pathways, which may be driven by multiple effectors. Rho-associated coiled−coil kinase, ROCK, is one of the most important Rho effectors and is essential for the formation of contractile actomyosin fibers (*14*).

Two isoforms of ROCK have been identified to date, ROCK I and ROCK II. The isoforms exhibit high sequence homology (about 65% identical amino acid residues and >90% similarity if conservative substitutions are counted). Both isoforms are ubiquitously expressed in most tissues with the exception of brain tissues, where ROCK II is predominant. ROCK phosphorylates and controls the activity of a number of proteins, such as MLC (*15*), MLC phosphatase, LIM kinase, ERM proteins, and Na^+-H^+ exchangers (*16*), all of which are essential players in cyctoskeleton organization. The conditional in vivo activation of ROCK has been shown to induce tumor cell dissemination and angiogenesis (*10, 17*). Fasudil, an approved drug for cerebral vasospasm, and Y-27632 are two small-molecule inhibitors of ROCK that have been used extensively in biochemical and pharmacological experiments to delineate the biological role of ROCK (*18*−*21*). Ischemia and reperfusion injuries result in Rho-ROCK activation leading to the recruitment of neutrophils and the generation of reactive oxygen species. Rats administered with Y-27632 1 h prior to ischemic reperfusion injury showed improved liver function and tissue protection (*19*). Administration of fasudil in water over a period of 5

* Corresponding author. Tel: (617) 444-6769. Fax: (617) 444-6105. Email: pazhanisamy@vrtx.com.

[1] Abbreviations: 5-HT, 5-hydroxytryptophan; AMPPNP, β,γ-imidoadenosine 5′-triphosphate; AMPPCP, β,γ-methyleneadenosine 5′-triphosphate; CSK, cSrc kinase; DTT, dithiothreitol; ERM proteins, ezrin/radixin/moesin proteins; HEPES, (*N*-[2-Hydroxyethyl]piperazine-*N*′-[2-ethanesulfonic acid]); LDH, lactate dehydrogenase; LIMK 1, LIM kinase 1; MAPKAP K2, MAP kinase activated protein kinase 2; MLC, myosin light chain; NADH, nicotinamide adenine diphosphate; PEP, phosphoenolpyruvate; PK, pyruvate kinase; PKA, protein kinase A; PKB, protein kinase B; ROCK, Rho associated coiled−coil kinase; S6AA peptide, AKRRRLAALRA; Y-27632, (*R*)-(+)-*trans*-4-(1-aminoethyl)-*N*-(4-pyridyl)cyclohexanecarboxamide dihydrochloride.

10.1021/bi052468q CCC: $33.50
Published on Web 06/06/2006

months to spontaneously hypertensive rats decreased the phosphorylation of the MLC phosphatase subunit and reduced the medial thickening of the aorta compared to those in the normotensive rats (*21*). Therefore, ROCK inhibitors have great therapeutic potential as disease modifiers by regulating the signaling via Rho-GTPase.

Interest in designing more potent and specific inhibitors of ROCK has resulted in the extensive characterization of its structure and function. ROCK I and II are approximately 160 kDa in size and contain the kinase domain in the *N*-terminus. There is a large segment of a coiled−coil region in ROCK, facilitating protein−protein interactions. The Rho binding domain is in the *C*-terminal end of the coiled−coil region and is followed by a plekstrin homology domain with cysteine-rich domain insertion (*22*). Recently, it was shown that full-length ROCK exists as a dimer in solution. Progressive *C*-terminal truncations up to R415 had no effect on either the kinase activity or the dimeric state of ROCK (*23*). The present mechanistic investigation utilizes truncated ROCK I (6−543), which was previously characterized to have activities similar to that of full-length ROCK. A previous study of ROCK II with a similar sized protein reported a random binding mechanism from the analysis of substrate and ATP analogue kinetics (*24*). Here, in addition to steady-state inhibition kinetics, we also used isotope partitioning techniques, K_d measurements of enzyme−inhibitor complex formation, viscosity effect on kinetic parameters, and presteady-state kinetics to probe the binding mechanism and catalysis by ROCK I. We observed that a strict interpretation of steady-state inhibition kinetics could be misleading at times and that additional methods such as isotope partitioning were necessary to validate the binding mechanism. Our investigation showed that the substrates bind randomly to ROCK I, as was the case for ROCK II. However, the binary complexes are not in rapid equilibrium with the central ternary complex. Also, the transfer of phosphate to the peptide occurs faster than the subsequent release of products, and hence, the rate-limiting step is one of product release associated with a possible conformational change in the enzyme.

MATERIALS AND METHODS

Materials. PEP, NADH, PK, and LDH were purchased from Roche diagnostics (Indianapolis, IN). ADP, ATP, AMPPNP, AMPPCP, and DTT were purchased from the Sigma Chemical Company (St. Louis, MO). Talon TM resin was from Clontech (Palo Alto, CA), thrombin was from Calbiochem (San Diego, CA). Peptides **1**−**3** were synthesized in-house. Peptides **4**−**8** and S6AA peptide were purchased from the American Peptide Company (Sunnyvale, CA).

Purification of ROCK I. The expression and purification of recombinant ROCK I was performed according to Doran et al. (*23*). Briefly, the kinase domain of human ROCK I (S6-L553) (*25*) was cloned into pBEV (custom dual-promoter bacterial expression and baculoviral transfer vector) for the baculo virus expression of His-tagged protein in High Five insect cells (Invitrogen, Carlsbad, CA). The protein was purified according to the following procedure. Typically, 40−60 g of the frozen cells were thawed and re-suspended in 5 volumes of buffer A (50 mM HEPES at pH 8.0, 100 mM NaCl, 2 mM β-mercaptoethanol, 10% glycerol). After the mechanical disruption of the cells in a microfluidizer (Microfluids Corp., Newton, MA), the lysate was centrifuged at 43 000*g* for 1 h. Imidazole (to 5 mM) and Talon TM resin (1:200 v/v) were added to the supernatant. The resin was washed with 10 volumes of buffer A plus 1 M NaCl and 5 mM imidazole and poured into a column. Bound histidine-tagged ROCK I protein was eluted with buffer A containing 100 mM imidazole. The tag was removed by incubation with thrombin (2 units/mg of protein) for 3 h at room temperature. When proteolysis appeared to be complete, as judged by SDS−PAGE analysis, thrombin was removed by incubating the solution with 100 μL of benzamidine sepharose for 30 min. ROCK I was then concentrated to 2 mL and loaded onto a 16/60 Sephadex S-200 column equilibrated with buffer A. The ROCK I protein eluted as a single peak, which was pooled, concentrated (typically around 1 mg/mL), and frozen at −80 °C until needed. At this stage, the protein appeared to be greater than 99% pure as judged by SDS−PAGE analysis. After thrombin cleavage, three amino acid residues (G, S, and H[2]) from the tag sequence remained on the *N*-terminus of the recombinant ROCK I protein, as confirmed by protein sequencing.

Kinase Assay. The coupled-enzyme assay, previously described by Chen et al. (*26*), was used to follow the initial rates of ROCK I-catalyzed reactions. The assays were carried out in 96-well plates. The assay conditions are as follows: 0.1M HEPES buffer (pH 7.6) containing 10 mM $MgCl_2$, 2.5 mM PEP, 0.2 mM NADH, 30 μg/mL of PK, 10 μg/mL of LDH, and 2 mM DTT. The kinase reaction was started by the addition of a substrate, either peptide or ATP, after a 10 min preincubation at 30 °C and read at 340 nm at 30 °C on a SpectraMax spectrophotometer (Molecular Devices Corp., Sunnyvale, CA). The concentration of the ROCK I enzyme was, unless otherwise indicated, 100 nM. Y-27632 and K252a were dissolved in DMSO and assayed at a final DMSO concentration of 2.5%. DMSO showed no significant effect on ROCK I activity at this concentration. The kinetic data were globally fitted to appropriate equations specified in the results section by nonlinear least-squares analysis using the software Prism, version 3.0 or 4.0 (San Diego, CA).

*Trapping [ROCK*ATP] Complex*. ROCK (1.67 μM) and ^{33}P-γ-ATP (5 μCi/nmole; 25 μM) were mixed in the kinase buffer to a final volume of 300 μL. Separately, 12.5 mM ATP and 1.25 mM of peptide **5** were mixed in the same buffer. A 200 μL of an aliquot of ATP/peptide **5** mix was added to the ROCK/^{33}P-ATP solution set at constant stirring. At approximately 30 s intervals, 50 μL of aliquots of the reaction mixture were withdrawn and quenched with 50 μL of 750 mM phosphoric acid. The quenched samples were analyzed in triplicate as follows: 25 μL of an aliquot of the quenched sample was placed on a P81 filter plate (cat. # MAPHNOB50, Millipore), vacuum filtered, and washed three times with 5% phosphoric acid, and 60 μL of Ultima Gold scintillant was added and the plate read for radioactivity on a Packard TopCount NXT counter.

Effect of Solvent Viscosity on Kinetic Constants. Assays were carried out under steady-state conditions as described above in HEPES buffer at pH 7.6 containing either sucrose

[2] The single letter code for each amino acid is used.

Table 1: Peptide Substrate Specificity for the ROCK I-Catalyzed Kinase Reaction

peptide	sequence	peptide K_m (μM)[a]	ATP K_m (μM)[b]	k_{cat} (s^{-1})	k_{cat}/K_m ($mM^{-1}\,s^{-1}$)[c]
1	KKPDKKKRYTVVGNPYWMA	<10	1.1		
2	KKRYTVVGNPYWMA	<10	1.3		
3	AKRRRLSSLRA	<10	1.5		
4	RRRLSSLRA	14.0 ± 1.7	15.0 ± 0.8	0.8 ± 0.02	57.1 ± 0.12
5	KKRNRTLSV	56.0 ± 3.3	9.0 ± 1.1	0.98 ± 0.02	17.5 ± 0.06
6	KKLRRTLSVA	57 ± 3	8.4 ± 0.5	0.92 ± 0.05	15.9 ± 0.05
7	KKVNRTLSVA	62 ± 7.7		0.5 ± 0.02	8.0 ± 0.13
8	LRRASLG	75 ± 6.6	7.5 ± 0.5	0.6 ± 0.02	8.1 ± 0.09

[a] ATP concentration was 2 mM. [b] Peptide concentration was 1 mM. [c] The peptide K_m values were used in the calculation.

(0−30%) or PEG-8000 (0−4%). An Ostwald viscometer was used to measure the time, *t*, taken by the experimental solution of density ρ to travel a fixed distance marked on the viscometer. The relative solvent viscosity (η^{rel}) was calculated from the equation (*27*), $\eta^{rel} = (t/t_0)(\rho/\rho_0)$, where t_0 and ρ_0 are values for the buffer without the added visocogen (sucrose or PEG-8000).

Presteady-State Kinetics. The presteady-state kinetics experiments were carried out in a chemical quench flow instrument, QFM5, Bio-Logic Instruments, France. As many as four reagents can be mixed (one being the chemical quench) and the flow-rate of each reagent controlled individually. There are two loops in the flow path, loop1 and loop2, whose lengths can be varied by installing appropriately sized loops. Reagents 1 and 2 mix into loop1 and reagent 3 enters this mix at loop2. The chemical quench in the fourth syringe enters at the end of loop2. This design allows the reaction time for reagents 1 and 2, and reagents 1,2, and 3, respectively, to be varied independent of each other. In addition, the instrument can be operated in a continuous mode or an interrupt mode. In the continuous mode, the reagents are pushed continuously for each run. The flow is diverted from the waste syringe to the collect syringe at a user specified time. Here, the reaction time is controlled by the loop size and the flow-rate. In the interrupt mode, the flow is interrupted for some specified length of time after the initiation of the reaction. This permits aging to occur for up to several seconds. However, in this method, the collectable sample volume is restricted to what is present in loop2. Because there is a possibility of contamination at either end of the loop due to diffusion, it is recommended that only the middle 2/3 of its contents be collected. We carried out the reaction in the continuous mode with loop sizes of 20, 100, and 200 μL at loop2. ROCK I (1.67 μM), ^{33}P-γ-ATP (100 μM), peptide **5** (2000 μM), and 10% TFA were placed in syringes 1, 2, 3, and 4, respectively. A 200 μL loop was used at loop1. The quenched samples were analyzed on an HPLC (Agilent-1100) equipped with a Packard radioactivity detector.

RESULTS

Substrate Screening. ROCK phosphorylates a number of proteins (*14*) in vivo and has a preference for substrates with a consensus sequence of either R/KXS/T or R/KXXS/T, where R is arginine, K is lysine, X is any amino acid, and S and T are serine and threonine, respectively (*14*). To choose an optimal phosphoryl acceptor for kinetic investigation, we designed and tested eight peptides on the basis of the known phosphorylation sites and sequence requirements. The peptides and their associated kinetic parameters are shown in Table 1. Peptides **1** and **2** are based on the phosphorylation site of LIMK1. The remaining peptides were included in the screen on the basis of sequence preference. Peptide **3** and **4** are S6 kinase substrates (*28*), peptides **5** and **6** were originally tried as PKB substrates (*29*), peptide **7** is a MAPKAP K2 substrate (*30*), and Peptide **8**, Kemptide, is a known substrate for PKA (*31*). The preliminary estimates of the kinetic parameters reveal that almost all peptides had nearly the same k_{cat} values (Table 1). The K_m values for peptides **1**−**3** were <10 μM and, therefore, were not considered suitable for the initial rate kinetic investigation because a low spectrophotometric signal would lead to considerable error in rate measurements at peptide concentrations below K_m. Most of the kinetics were, therefore, carried out with peptide **5**, and in a few studies, peptide **8** was used.

Bisubstrate Kinetics. The initial rates of ROCK I-catalyzed phosphorylation of peptide **5** were determined over a range of concentrations of the peptide and ATP. The reciprocals of the rates were plotted as a function of the inverse of ATP (Figure 1A) and peptide **5** concentrations (Figure 1B). Both sets of lines intersect at the lower left quadrant indicating a sequential mechanism. Peptide **8** also gave a similar kinetic pattern (data not shown). The data were fitted to eq 1, where v, V, A, and B are initial velocity, maximum velocity, the concentration of ATP, and the concentration of peptide, respectively. K_{ia} is the dissociation constant for A from EA, and K_a and K_b are the K_m values for A and B, respectively[3]. The kinetic parameters thus evaluated are presented in Table 2.

$$v = \frac{VAB}{K_{ia}K_b + K_bA + K_aB + AB} \quad (1)$$

Inhibition by an S6AA Peptide. Replacement of the phosphorylatable serines with alanine in the S6 peptide (peptide **3** in Table 1) yields the S6AA peptide, which inhibits enzyme activity and, hence, should be competitive with substrate binding. Initial rates were obtained in the presence of various fixed concentrations of the inhibitor peptide by varying either the peptide substrate or ATP while keeping the other constant. A plot of the reciprocals of the rates as a function of the inverse of peptide concentration yielded the expected competitive inhibition pattern (Figure 2A), whereas it gave a noncompetitive pattern (Figure 2B)

[3] Cleland nomenclature; Cleland, W. W. (1970) Steady-state kinetics, in *The Enzymes* (Boyer, P. D., Ed.) 3rd ed., Vol. 2, pp 1−65. Academic Press, New York.

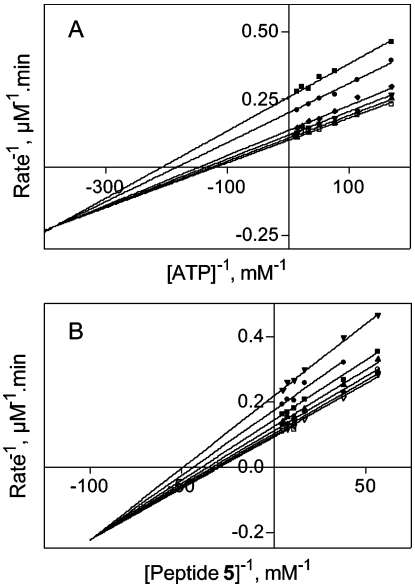

FIGURE 1: Substrate kinetics for the ROCK I-catalyzed kinase reaction. Peptide **5** was used as a phosphoryl acceptor. The initial rates (v) were obtained by the spectrophotometric assay as described in the Materials and Methods section. A matrix of initial rates were obtained as a function of ATP (5.9, 8.8, 13.2, 19.8, and 44.4 μM) and peptide **5** (17.6, 26.3, 59.3, 88.9, 133.3, and 200 μM) concentrations at 30 °C in 0.1 M HEPES buffer (pH 7.6) containing 10 mM $MgCl_2$ and 2 mM DTT. ROCK I concentration was 200 nM. The plots of the data either as $1/v$ vs 1/[ATP] (Panel A) or $1/v$ vs 1/[peptide **5**] (Panel B) yielded intersecting patterns. The solid lines represent the best global fit of the data to eq 1, and the best-fit values are presented in Table 2.

Table 2: Kinetic Parameters for the ROCK I-Catalyzed Kinase and ATPase Reactions

parameter	kinase[a]	ATPase
k_{cat} (s^{-1})	1.05 ± 0.03	0.05 ± 0.01
K_{ATP} (μM)	9.4 ± 0.8	3.9 ± 0.1
$K_{ia,ATP}$ (μM)	2.6 ± 0.6	
K_{Pep} (μM)	36.6 ± 2.8	
$K_{ia,Pep}$ (μM)	10.2 ± 2.3	
α (= K_{ATP}/K_{ia})	3.6 ± 0.8	

[a] The bisubstrate kinetics were performed with peptide **5**, KKRNRTLSV, and the data were fitted to eq 1.

for ATP dependence. The competitive inhibition data were fitted to eq 2, and the noncompetitive inhibition data were fitted to eq 3, where S is the concentration of the varied substrate (ATP or peptide); K_{is} and K_{ii} are the inhibitor dissociation constants for dissociating from the EI and ESI complexes, respectively (Table 3).

$$v = \frac{VS}{K_m(1 + I/K_{is}) + S} \quad (2)$$

$$v = \frac{VS}{K_m(1 + I/K_{is}) + S(1 + I/K_{ii})} \quad (3)$$

Inhibition by ATP Analogues, Y-27632, and K252a. The small-molecule inhibitors Y-27632 and K252a and the ATP analogues, AMPPNP and AMPPCP, are competitive inhibitors of ATP (the rate was obtained as a function of multiple ATP and inhibitor concentrations; data not shown) and their respective K_{is} values were obtained from the kinetic data

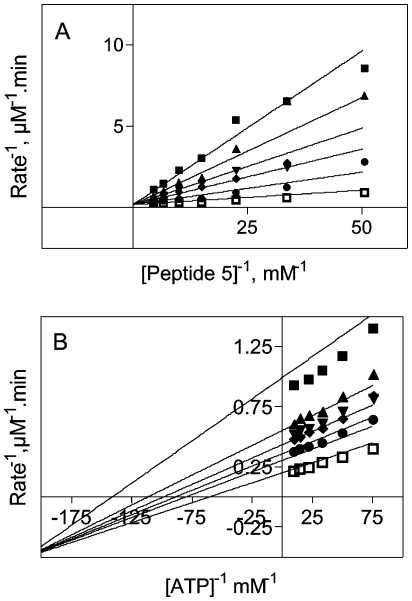

FIGURE 2: Inhibition kinetics with peptide inhibitor, S6AA. (A) ATP concentration was fixed at 45 μM, whereas the concentration of the peptide **5** was varied (20−225 μM) in the presence of various fixed concentrations of S6AA (0, 0.26, 0.59, 0.89, 1.33, and 2.0 mM). The solid lines are the best global fit of data to eq 2 for the competitive inhibition model. (B) The concentration of peptide **5** was fixed at 200 μM, whereas the concentration of ATP was varied (9−100 μM) in the presence of various fixed concentrations of S6AA (0, 0.26, 0.4, 0.59, 0.89, and 2.0 mM). The solid lines are the best fit of the data to eq 3 for the noncompetitive inhibition model. The best-fit values for K_{is} and K_{ii} are presented in Table 3.

Table 3: Kinetic Parameters for the Inhibition of ROCK I-Catalyzed Kinase Reaction

varied substrate	inhibitor	inhibition pattern[a]	K_{is} (μM)	K_{ii} (μM)
ATP	AMP-PNP	C	33 ± 3	
peptide **5**	AMP-PNP	UC		130 ± 20
peptide **8**	AMP-PNP	UC		52 ± 4
ATP	AMP-PCP	C	150 ± 12	
peptide **3**	AMP-PCP	UC		357 ± 31
peptide **5**	AMP-PCP	UC		596 ± 29
peptide **8**	AMP-PCP	UC		500 ± 28
ATP	Y27632	C	0.15 ± 0.03[b]	
peptide **8**	Y27632	UC		0.40± 0.08
ATP	K252a	C	0.42 ± 0.05	
peptide **5**	K252a	NC	1.28 ± 0.37	0.60 ± 0.14
ATP	S6AA	NC	1780 ± 1290	510 ± 90
peptide **5**	S6AA	C	207 ± 81	

[a] The data were fitted to either eq 2 (competitive pattern, C), eq 3 (noncompetitive pattern, NC), or eq 5 (uncompetitive pattern, UC).[b] The data were fitted to eq 4. See the Materials and Methods section for details.

(Table 3) by global fitting to eq 2. The data for Y-27632 was fitted to eq 4 (*32*) because the free inhibitor concentration can be significantly less than the total. Here, v_0 is the rate in the absence of the inhibitor, E_t and I_t are the total enzyme and inhibitor concentrations, respectively, and $K_{i,app}$ is $K_i(1 + [ATP]/K_m)$. These compounds were also assayed as a function of peptide **5** in the kinase assay. The resulting reciprocal plots are shown in Figure 3A−C.The ATP analogues and Y-27632 yielded a set of lines that appear parallel and were best fit to a model of uncompetitive inhibition (eq 5); the resulting K_{ii} parameters are shown in

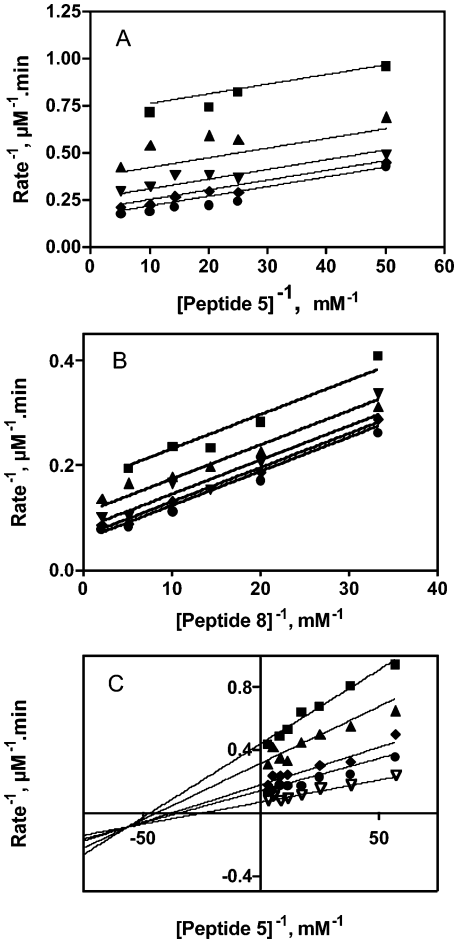

FIGURE 3: Inhibition kinetics with AMPPNP, Y-27632 and K252a. (A) ROCK I concentration was 200 nM. ATP concentration was fixed at 30 μM, whereas the concentration of peptide **5** was varied (20−200 μM) in the presence of various fixed concentrations of AMPPNP (0, 20, 50, 100, and 200 μM). (B) ATP concentration was fixed at K_m, whereas the concentration of peptide **8** was varied (20−500 μM) in the presence of various fixed concentrations of Y-27632 (0, 0.125, 0.25, 0.5, and 1.0 μM). (C) ATP concentration was fixed at 45 μM, whereas the concentration of peptide **5** was varied (17−300 μM) in the presence of various fixed concentrations of K252a (0, 0.59, 0.89, 0.2.0, and 3.0 μM). The data in panels A and B were treated as uncompetitive inhibition and globally fitted to eq 5, whereas the data in panel C were fitted to eq 3 for noncompetitive inhibition. The best-fit values for K_{is} and K_{ii} are presented in Table 3.

Table 3. The staurosporine analogue K252a, however, yielded intersecting lines, and therefore, the data were fitted to eq 3 for noncompetitive inhibition.

$$v = \left(\frac{v_0}{2E_t}\right)\{(E_t - I_t - K_{i,app}) + \sqrt{(E_t - I_t - K_{i,app})^2 + 4E_tK_{i,app}}\} \quad (4)$$

$$v = \frac{VS}{K_m + S(1 + I/K_{ii})} \quad (5)$$

ATPase Activity of ROCK I. ROCK I hydrolyzes ATP in the absence of peptides. The ATPase activity was weak but at 0.5 μM ROCK I yielded a saturation curve (Figure 4A). The K_m value for ATP is 4 μM, and the k_{cat} value is 0.05 s^{-1}

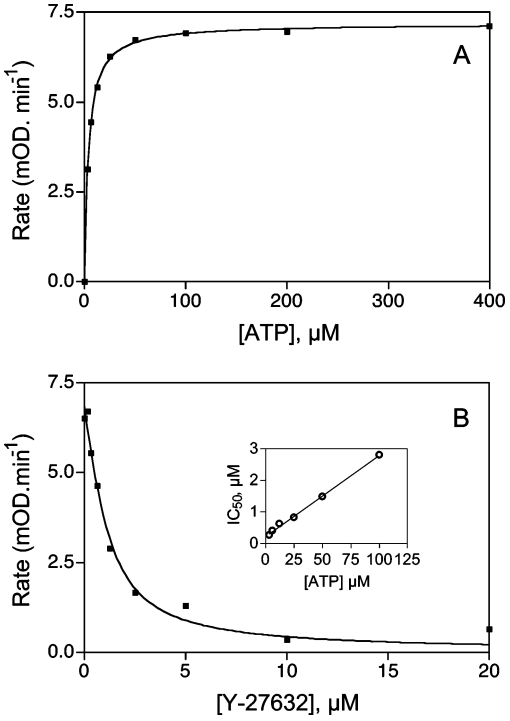

FIGURE 4: ATPase activity of ROCK I and its inhibition by Y-27632. The ADP generated by ATPase activity was followed by the spectrophotometric assay as described in Materials and Methods. (A) At 0.5 μM ROCK I, the initial rates were obtained as a function of ATP concentration. The data were fitted to Michelis−Menton kinetics. (B) At a fixed concentration of ATP (15 μM), the ATPase activity was assayed as a function of Y-27632 concentration. The data were fitted to eq 4 for tight-binding competitive inhibition kinetics to evaluate the K_i value. The IC_{50} value for inhibition was also obtained as a function of ATP concentration (3−100 μM) and is presented as an inset. The K_i value was evaluated by fitting the data to eq 6.

(Table 2). ATPase activity was also inhibited by Y-27632 (Figure 4B). The IC_{50} value of inhibition increased linearly as a function of increasing ATP concentrations (Figure 4B, inset), which is diagnostic of competitive inhibition (*33*). The IC_{50} versus [ATP] data was fitted to eq 6, which is applicable to competitive inhibition kinetics, where the enzyme concentration is comparable to the inhibitor concentration. The fit yielded a K_i value of 0.11± 0.03 μM, which is similar to the K_i value for the inhibition of the kinase activity of ROCK by Y-27632 (Table 3).

$$IC_{50} = \frac{E_t}{2} + K_i\left(1 + \frac{[ATP]}{K_m}\right) \quad (6)$$

K252a Binding to ROCK I. Upon excitation at 300 nm, K252a fluoresced with two distinct emission bands centered at 380 and 396 nm. The intensities of both bands enhanced upon its binding to ROCK I. By fixing the concentration of K252a at 200 nM, the change in emission intensity at 380 nm was monitored as a function of ROCK I concentration (Figure 5). The titration data were fitted to eq 7 (*34*), where ΔF is the increase in fluorescence, $\Delta\epsilon$ is the change in the molar extinction coefficient upon binding, K_d is the dissociation constant, and Eo and Lo are the nominal concentrations

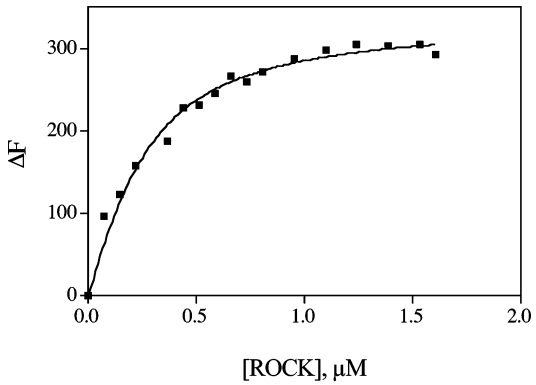

FIGURE 5: Fluorescence titration of K252a binding to ROCK I. To a 200 μL solution of 200 nM K252a in 0.1 M HEPES buffer at pH 7.6, 20 μM ROCK I was added as 1μL aliquots. K252a was excited at 300 nm, and the emission spectrum was recorded from 300 to 400 nm. The change in Fluorescence at 380 nm as a function of ROCK I concentration was fitted to eq 7 to evaluate the K_d value.

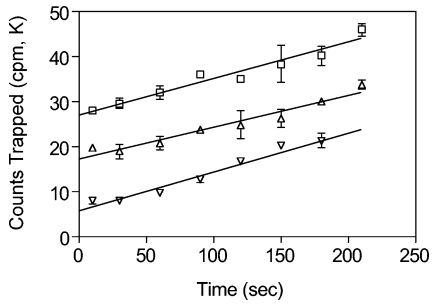

FIGURE 6: ROCK−ATP complex is a viable intermediate in the kinase reaction. A pulse solution containing ROCK I (1.67 μM) and ^{33}P-ATP (25 μM) was mixed with the chase solution containing ATP (10 mM) and peptide **5** (500 μM) in the ratio 3:2 maintained at a constant stirring. Aliquots were drawn at various reaction times and quenched with phosphoric acid (750 mM), and the phosphopeptide product was quantified as described in the Materials and Methods section. The concentration of Y-27632 in the pulse was either 0 (□), 1.5 (△), or 10 μM (▽). The slopes and intercepts were evaluated from a linear fit of the data.

of ROCK I and K252a, respectively. The fit yielded a value of 0.15 μM for the dissociation constant, K_d.

$$\Delta F = (\Delta\epsilon/2)[(K_d + \mathrm{Eo} + \mathrm{Lo}) - ((K_d + \mathrm{Eo} + \mathrm{Lo})^2 - 4\mathrm{EoLo})^{1/2}] \quad (7)$$

Isotope Partitioning. The kinetic competence of the [ROCK−ATP] complex in the kinase reaction can be evaluated by an isotope partition experiment (*35*). A pulse of a ROCK (1.67 μM) solution containing ^{33}P-γ-ATP (25 μM) was diluted into a continuously mixed chase solution with a large excess of unlabeled ATP (10 mM) and 0.5 mM peptide **5** in the ratio 3:2. Aliquots were drawn as a function of time and quenched with equal volumes of 5% phosphoric acid. The labeled phosphopeptide product in the quenched sample was quantified as detailed in the Materials and Methods section. The radioactivity counts in the phosphopeptide as a function of time is presented in Figure 6. The intercept corresponds to 1.10 ± 0.17 μM of phosphopeptide product[4], which amounts to trapping 66% [= (1.10/1.67)*100] of the E−ATP in the pulse assuming that ATP was at saturating concentration. The slope of the line corresponds to the steady-state turnover of the enzyme at V_{max} conditions. From the slope, a k_{cat} value of 1.0 ± 0.2 s^{-1} was obtained, which agreed well with the data for bisubstrate kinetics. To ensure that the counts trapped were not due to nonspecific binding artifacts, an ATP competitive inhibitor, Y-27632, was added to the pulse. The addition of 1.5 and 10 μM Y-27632 in the pulse decreased the intercept as a function of its concentration but had no significant effect on the slope.

Effect of Solvent Viscosity on Kinetic Parameters. Physical processes such as diffusion and conformational changes can be affected by the presence of a microviscogen such as sucrose, whereas chemical changes, bond-breaking, and bond-making, are not affected (*36*). A macroviscogen (e.g., PEG-8000), however, has no significant effect on either process. Therefore, the effect of a microviscogen on kinetic parameters is a powerful tool to probe the nature of the rate-limiting event. Michelis−Menten kinetics were performed in solvents of differing viscosity, containing either micro or macroviscogens, to obtain k_{cat}/K_m values for ATP and k_{cat} by keeping the peptide concentration fixed at saturation (peptide = 1 mM). The ratio of the kinetic parameter obtained in the presence of the viscogen (k_η) to the one in its absence (k_o) was plotted against the relative viscosity of the medium (η^{rel}). The slope from the linear fit of the data yields the viscosity effect on the kinetic parameter. The top and bottom panels in Figure 7 present the viscosity effect on the k_{cat}/K_m value for ATP and k_{cat}, respectively, as a function of the relative viscosity of the medium. The effect on the k_{cat}/K_m value for the peptide (ATP = 1 mM) is represented in the middle panel. The viscosity effects derived from the slopes of the lines are presented in Table 4. The viscosity effect on the k_{cat} value is 1.3 ± 0.2 in sucrose medium. Because there is a nonspecific effect of 0.3 ± 0.1 on k_{cat} in PEG-8000, the net viscosity effect can be considered to be 1. By the same token, the net viscosity effect on the k_{cat}/K_{pep} value is also unity. The net viscosity effect on the k_{cat}/K_{ATP} value, however, is slightly greater than 1 for which we do not have an explanation.

Presteady-State Kinetics. The kinetic parameters determined from steady-state kinetics often represent a composite of rate constants. To measure the rate constants of individual steps, one has to resort to presteady-state kinetics (*37*). We carried out presteady-state kinetics at saturating concentrations of ATP and peptide using the rapid chemical quench flow technique. The enzyme, ^{33}P-γ-ATP, and the peptide were kept in separate syringes and were mixed in a 1:1:1.2 ratio. After allowing the reaction to proceed for a specified length of time, TFA (10%) in the fourth syringe was added to quench the reaction. The phosphopeptide content of the quenched sample was analyzed by HPLC equipped with a radioactivity detector. The phosphopeptide produced (expressed as a mole fraction of ROCK I in the assay) as a function of reaction time is plotted in Figure 8. The kinetics is biphasic with an initial burst phase followed by a linear phase. The data were fitted (*37*) to eq 8, where k_b is the rate constant for the burst phase, L is the slope of the linear phase, A is the amplitude of the burst, and Y is the concentration of the phosphopeptide product expressed as a mole fraction of enzyme in the assay at a given time t. The fit yielded a value of 10.2 ± 2.1 s^{-1} for k_b, and the slope L corresponded to a

[4] Average of three separate determinations.

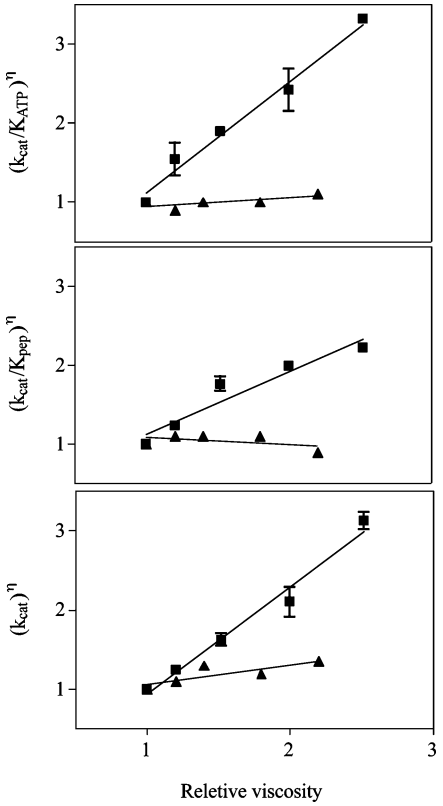

FIGURE 7: Effect of viscosity on the ROCK I-catalyzed kinase reaction. The k_{cat} and the K_m values for ATP (varied concentrations 1.56−200 μM; keeping peptide **5** at 500 μM) and peptide **5** (varied concentrations 3.9−500 μM; keeping ATP at 200 μM) were obtained as a function of relative viscosity. The ratio of k_{cat}/K_m in the absence of added viscogen over that in its presence is plotted as a function of relative viscosity in the top and middle panels for ATP and peptide **5**, respectively. In the bottom panel, the ratio of k_{cat} values is plotted as a function of relative viscosity. Data obtained in the presence of the microviscogen (sucrose), (■); macroviscogen (PEG-8000), (▲); the best linear fit of the data, (—). The slopes yield the viscosity effect and are presented in Table 4.

Table 4: Viscosity Effect on Kinetic Parameters

		viscosity effect	
parameter	varied substrate[a]	sucrose	PEG-8000
k_{cat}/K_{ATP}	ATP	1.4 ± 0.2	0.1 ± 0.1
k_{cat}/K_{Pep}	peptide	0.9 ± 0.3	−0.1 ± 0.1
k_{cat}		1.3 ± 0.2	0.3 ± 0.1

[a] The other substrate was kept at saturating concentration. See the Materials and Methods section for details.

turnover number of 0.9 ± 0.2 s^{-1}. The burst amplitude A was 1.02 ± 0.13.

$$Y = A\{1 - \exp(-k_b t)\} + Lt \quad (8)$$

DISCUSSION

Substrate Specificity. Full-length ROCK I is comprised of 1354 amino acid residues with the kinase domain in the *N*-terminus (76−338). The kinase domain is followed by a large coiled−coil region, which includes a short stretch called the Rho binding domain. We used recombinant ROCK I with the sequence S6-L553 in the mechanistic investigations and found the enzyme activity to be linear over the enzyme concentration range used in our studies (data not shown).

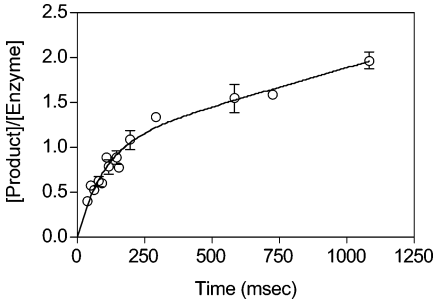

FIGURE 8: Pre-steady-state kinetics of ROCK I-catalyzed kinase reaction. ROCK (1.67 μM), ^{33}P-γ-ATP (100 μM), and peptide **5** (2 mM) were kept in separate syringes and mixed in the ratio 1:1:1.2 in the rapid mix unit, QFM5, Bio-Logic Instruments. The variously aged reactions (see Materials and Methods for details) were quenched with 10% TFA in syringe 4. The quenched samples were analyzed on HPLC to quantify the phosphopeptide product. The phosphopeptide product concentration (as a mole fraction of enzyme used in the assay) plotted against reaction time exhibits biphasic kinetics. The solid line represents the best fit of data to eq 8.

Scheme 1: Random Binding Mechanism for ROCK I-Catalyzed Kinase Reaction[a]

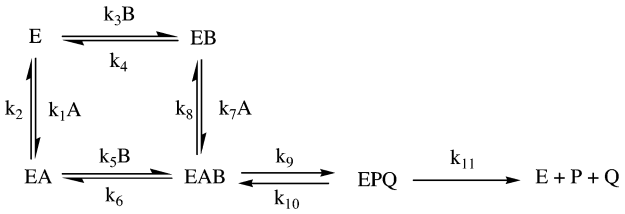

[a] E, A, B, P, and Q are ROCK I, ATP, peptide, phosphopeptide, and ADP, respectively.

ROCK I belongs to a subgroup of serine/threonine kinases possessing substrate specificity for a positive charge at −P3 or −P2 with respect to the site of phosphorylation. A number of peptides meeting the above criterion were tested, and all of them were found to be good substrates (Table 1). Interestingly, the turnover number (k_{cat}) is virtually the same for all, irrespective of peptide length and identity. The K_m value for ATP also did not change (≤2-fold) as much compared to the K_m value for the peptide substrates. For the mechanistic investigation, we used peptide **5**, and in some kinetic studies, peptide **8** was also used.

Kinetic Mechanism. Lineweaver−Burk plots of the bisubstrate kinetic data (Figure 1A and B) show a family of lines intersecting in the bottom left quadrant. This kinetic pattern is certainly inconsistent with a ping−pong mechanism, which has no precedence in serine/threonine or tyrosine protein kinase literature. For a sequential binding mechanism in which the substrates bind randomly (Scheme 1), this pattern would suggest negative cooperativity between the substrates, that is, the affinity is less for a substrate to form a ternary complex with the enzyme in binary complex (with the other component) than for binding to the free enzyme to form a binary complex. The nonphosphorylatable S6AA peptide showed the expected competitive inhibition kinetics with the peptide substrate but noncompetitive kinetics with ATP (Figure 2A and B). ATP analogues, AMPPNP and AMPPCP, and the ATP-competitive inhibitor Y-27632 all showed an uncompetitive pattern when the peptide was the varied substrate (Figure 3; data not shown for AMPPCP), while

exhibiting a competitive pattern with ATP (Table 3). These observations suggest a specified order of binding, that is, peptide binds first. This is intriguing in that most kinases were reported to follow a random binding order, and in a few cases, ATP was the first substrate to bind. Also, the limited mechanistic data available for ROCK II supports a random binding mechanism (*24*). It would be unusual for two isozymes of high homology (>90%) to exhibit different kinetic behaviors. Also, K252a, a staurosporine analogue, yielded a noncompetitive inhibition kinetics pattern versus the peptide substrate (Figure 3C), which is consistent with the random binding order. Examples of substrate analogues exhibiting differing patterns of inhibition with the substrate are rare but have been documented. For glycerokinase, the inhibition kinetics was consistent with glycerol binding first. However, the order of binding appeared to be reversed, that is, ATP bound first, when (*S*)-mercaptoglycerol was used as a substrate (*38*). The bisubstrate kinetics showed a large synergism in binding, that is, it matters if the ligand is binding to the free enzyme or to a binary complex of enzyme. It was interpreted that the enzyme indeed is capable of binding one substrate in the absence of the other and, hence, utilizes the random binding mechanism but exhibits kinetics of a preferred order for specific substrates. The presence of ATPase activity was considered to be supporting evidence for the E−ATP binary complex in the kinase reaction. For MAPKAP K2, the substrate analogue and product inhibition kinetics were inconclusive. The surface plasmon resonance (SPR) studies clearly eliminated the existence of an E−peptide complex, and hence, the kinetic mechanism for MAPKAP K2 was concluded to be ordered binding, that is, ATP binds first (*39*).

Hence, for ROCK I, we decided to carry out experiments that could independently shed light on the binding mechanism. First, we sought to look for ATPase activity. The ATPase activity of ROCK I was weak but observable at high enzyme concentrations (Figure 4). The k_{cat} value was some 20-fold less than that of the kinase reaction (Table 2). More importantly, ATPase activity was inhibited by Y-27632 (Figure 4) with a K_i value of 0.11 μM. This value is similar to the K_i value of 0.15 μM for inhibiting kinase activity.[5] Also, the staurosporine analogue K252a, an ATP competitive inhibitor, exhibited enhanced fluorescence upon binding to ROCK I. The fluorescence titration (Figure 5) yielded a K_d value of 0.15 μM, which is again comparable to its K_i value for kinase inhibition (Table 3). The presence of ATPase activity and the direct binding of the ATP competitive inhibitor capable of blocking kinase activity clearly point to the existence of a productive E−ATP complex.

Isotope Partitioning. This is a powerful method to validate the presence of catalytically relevant intermediates in enzyme-catalyzed reactions (*35*). Kong and Cook successfully exploited this technique (*40*) to show unequivocally that PKA indeed utilizes a random binding mechanism as opposed to the ordered addition of substrates proposed earlier (*41*). In this method, to test the validity of the [ROCK−ATP] complex as an intermediate in the kinase reaction, ^{33}P-γ-ATP mixed with ROCK constituted the pulse, which was chased by a mixture consisting of a large excess of unlabeled ATP and saturating concentrations of peptide for the kinase reaction. If there were any productive E−^{33}P-γ-ATP complex present in the pulse, it would form a ternary complex with the peptide and yield a phosphopeptide product. The phosphopeptide produced in this first turnover will have a very high specific activity. In the subsequent turnovers, the specific activity of ATP gets diluted dramatically, and hence, the specific activity of the phosphopeptide product also goes down in the same proportion. However, the reaction was sampled at multiple time points, and we observed that the radioactivity incorporation into the product is linear with time (Figure 6). The interpolation to the *y*-axis (to time zero) yielded the counts trapped in the first turnover. As expected, the counts trapped in the subsequent turnovers were small compared to that from the first turnover. The intercept corresponded to 1.10 μM phosphopeptide product produced in the first turnover containing 1.67 μM ROCK. To ensure that the counts trapped were not due to artifacts such as nonspecific binding, an ATP competitive inhibitor Y-27632 was added to the pulse. This should reduce or eliminate the ROCK−ATP complex, depending upon the inhibitor concentration and, hence, should have a direct impact on the intercept. It is clear from Figure 6 that the intercepts were significantly reduced when the pulse contained 1.5 and 10 μM of Y27632 compared to the no inhibitor control. However, the slopes were largely unaffected because the unlabeled ATP concentration in the chase was great enough to overcome the impact of the added inhibitor.

In setting up this experiment, we assumed that the K_m value in the ATPase reaction (4 μM) is the K_d value for the ROCK−ATP complex. For 1.67 μM ROCK mixed with 25 μM ^{33}P-ATP in the pulse, 1.1 μM ^{33}P-phosphopeptide was formed. If we assume that all E−ATP binary complexes in the pulse were trapped, a K_d value of 12 μM can be calculated[6], which is in reasonable agreement with ATPase data. The calculated value provides the upper limit, that is, $K_d \leq 12$ μM. Nevertheless, the fact that a significant portion of the [E−^{33}P-ATP] complex could be trapped suggests that [E−ATP] is a kinetically viable intermediate. Therefore a random binding mechanism with both [E−ATP] and [E−Peptide] as viable intermediates best explains all of the kinetic data for ROCK I (Scheme 1).

The bisubstrate kinetic data of Figure 1 were accordingly fitted to eq 1 for a random binding mechanism, and the parameters thus evaluated are shown in Table 2. The K_d value for the [E−ATP] complex (K_{ia} in eq 1) is 2.6 μM, and the interaction parameter, α ($=K_{ATP}/K_{ia}$), for the negative cooperativity is 3.6. These values may justify why the data of Figure 3A and B appear to be parallel. First of all, eqs 2−4 are strictly applicable to a one substrate reaction. When applied to the bisubstrate reaction, the K_{is} and K_{ii} values obtained are a function of the fixed substrate concentration and the interaction parameter α. For the ATP competitive ligands of ROCK, the low K_{ia} value for ATP and the large

[5] One of the reviewers raised the question of whether Y-27632 is a slow-binding inhibitor. The following evidence suggests that it is not a slow-binding inhibitor. There is no downward curvature in the progress curves for the onset of inhibition or an upward curvature in the return of activity experiment. Also, the IC_{50} value for inhibition does not change with varying times of preincubation (up to 15 min) of ROCK I with Y-27632.

[6] Substituting 1.67, 1.1, and 25 μM for $[E]_o$, [E−ATP], and $[ATP]_o$, respectively, in $K_d = ([E]_o - [E-ATP])([ATP]_o - [E-ATP])/[E-ATP]$ yielded a value of 12.4 μM for the dissociation constant, K_d.

value for α predict the noncompetitive inhibition pattern of lines to intersect in the lower left quadrant just as they did in the absence of inhibitors in Figure 1 A and B. The use of a high ATP concentration relative to its K_{ia} value (because of the practical limitation in obtaining measurable rate) makes the K_{is} term much larger than K_{ii} (Table 3), and the lines, therefore, naturally tend to appear parallel. Additionally, if the inhibitor exhibits any preference for binding to the binary complex over the free enzyme (positive cooperativity for inhibitor binding as opposed to the negative cooperativity observed for substrate binding; interaction parameter $\beta < 1$), then the lines can also appear to be nearly parallel, leading to an erroneous interpretation (*42*).

Viscosity Effect on Kinetic Parameters. The steady-state kinetic parameters shown in Table 2 are of limited value in understanding catalysis because they represent a composite of many individual steps. Kinetic isotope effects, solvent viscosity effects on rate constants, and linear-free energy relationships are some of the techniques used to tease out the nature of the rate-limiting step from the steady-state turnover data of enzyme-catalyzed reactions. Although the presence of a kinetic isotope effect will normally identify the chemical step to be rate-limiting (*43*), the lack of a viscosity effect (*44*) would point to the same conclusion. The viscosity effect is defined as the fold decrease in the rate constant per unit change in the relative viscosity of the medium. The solvent viscosity effect on a composite rate constant ranges from 0 (insensitive) to 1 (fully sensitive). Physical processes such as the diffusion of reagents in and out of the active site or conformational changes associated with the enzyme can be affected by the viscosity of the medium (η). It is assumed that the viscosity effect on a given physical step is an all (= 1) or nothing (= 0) effect and has no intermediate sensitivity. Therefore, a viscosity effect of greater than zero but less than 1 on a kinetic parameter such as k_{cat}/K_m or k_{cat} is taken to mean that the chemical step as well as at least one solvent-sensitive physical step are rate-limiting steps for that process.

For the reaction in Scheme 1, which describes the ROCK kinase mechanism, the viscosity effects on the k_{cat}/K_m value for the peptide[7] and ATP are given by the eqs 9 and 10, respectively.

$$(k_{cat}/K_{pep})^{\eta} = \frac{k_9}{k_6 + k_9} \tag{9}$$

$$(k_{cat}/K_{ATP})^{\eta} = \frac{k_9}{k_8 + k_9} \tag{10}$$

The observed viscosity effect was 1, within error, for both k_{cat}/K_m parameters. Therefore, $k_9 \gg k_6$, k_8, that is, the binding steps, have higher barriers than the chemical step. In other words, once the ternary complex is formed, it is committed to go forward with the phosphoryl transfer, at least by a factor of 10, rather than revert back to the binary complex by releasing either ATP or the peptide. Therefore, at least at the level of second ligand binding, the substrates do not equilibrate among the enzymic species (Scheme 1) before the chemical event takes place. The fact that the chemical step is faster than the substrate release steps allows us to estimate the on-rate constants k_5 and k_7 directly from the k_{cat}/K_m values for ATP and the peptide, respectively (Table 5).

Table 5: Observed and Derived Kinetic Parameters for the ROCK I-Catalyzed Kinase Reaction

parameter	value	method of determination
k_{cat}	$1.05 \pm 0.03\ s^{-1}$	fit to eq 1; equals $k_9.k_{11}/(k_9 + k_{11})$
$K_{ia,ATP}$	$2.6 \pm 0.6\ \mu M$	fit to eq 1; equals k_2/k_1
K_{ATP}	$9.4 \pm 0.8\ \mu M$	fit to eq 1
$K_{ib,Pep}$	$10.2 \pm 2.3\ \mu M$	fit to eq 1; equals k_4/k_3
K_{Pep}	$36.6 \pm 2.8\ \mu M$	fit to eq 1
k_{cat}/K_{ATP}	$0.11 \pm 0.01\ \mu M^{-1}\ s^{-1}$	$= k_7k_9/(k_8 + k_9)$
k_{cat}/K_{Pep}	$0.029 \pm 0.002\ \mu M^{-1}\ s^{-1}$	$= k_5k_9/(k_6 + k_9)$
k_5	$\sim 0.11 \pm 0.01\ \mu M^{-1}\ s^{-1}$	$k_{cat}/K_{m,ATP}$ is $k_5k_9/(k_6 + k_9) \Rightarrow \sim k_5$
k_6	$<1\ s^{-1}$	viscosity data ($k_6 \ll k_9$)
k_7	$\sim 0.029 \pm 0.002\ \mu M^{-1}\ s^{-1}$	$k_{cat}/K_{m,Pep}$ is $k_7k_9/(k_8 + k_9) \Rightarrow \sim k_7$
k_8	$<1\ s^{-1}$	viscosity data ($k_8 \ll k_9$)
k_9	$10.2 \pm 2.1\ s^{-1}$	transient kinetics; fit to eq 8
k_{10}		
k_{11}	$1.05 \pm 0.03\ s^{-1}$	viscosity data ($k_{cat} \sim k_{11}$)

The k_{cat} value is a composite of any and all rate constants associated with steps starting from the ternary complex E−ATP−peptide to the regeneration of the free enzyme. In Scheme 1, the product release steps and any other distinct conformational change associated with the product release are all grouped into one single step, k_{11}. We assumed that the chemical step is essentially irreversible, though this will be justified later. Then, the viscosity effect on k_{cat} is given by eq 11

$$(k_{cat})^{\eta} = \frac{k_9}{k_9 + k_{11}} \tag{11}$$

Here again, the observed viscosity effect is near unity (Table 4) implying $k_9 > k_{11}$. Thus, the k_{cat} value of $1\ s^{-1}$ may correspond either to a product release step or, alternatively, to a conformational transition of the enzyme along the way (all included in k_{11}). Also, it follows that the phosphoryl transfer step should be at least 10 times faster than k_{11}.

Presteady-State Kinetics. The viscosity effects predicted the phosphoryl transfer step to be much faster than the product release steps and offered the lower limit for the phosphoryl transfer rate constant ($k_9 \geq 10\ s^{-1}$). A better estimate for k_9 can be obtained from rapid reaction kinetics. Quench flow kinetics under saturation conditions of substrates yielded biphasic kinetics (Figure 8). The burst phase corresponds to the accumulation of enzyme-bound product species. Fitting the data to eq 8 yielded a value of $10.2 \pm 2.1\ s^{-1}$ for the burst-phase rate-constant, $0.9 \pm 0.2\ s^{-1}$ for the steady-state rate-constant, and 1.02 ± 0.13 for the burst amplitude. The

[7] Because $(k_{cat}/K_{pep}) = k_5k_9/(k_6 + k_9)$, the viscosity effect expression for k_{cat}/K_{pep} is given by $\left(\frac{k_{cat}}{K_{pep}}\right)^{\eta} = \frac{\left(\frac{k_{cat}}{K_{pep}}\right)_0}{\left(\frac{k_{cat}}{K_{pep}}\right)_{\eta}} = \left(\frac{k_5}{k_{5\eta}}\right)\left(\frac{k_9 + k_{6\eta}}{k_9 + k_6}\right)$, where the subscript η represents the value of the parameter obtained in the presence of the viscosity agent. If the physical step was rate-limiting ($k_9 \gg k_6$, $k_{6\eta}$), then the right-hand side (RHS) reduces to $k_5/\ k_{5\eta}$, which is equal to η^{rel}. Hence, it will yield a slope of 1 when plotted against the relative viscosity, η^{rel}. For a rate-limiting chemical step ($k_9 \ll k_6$, $k_{6\eta}$), the RHS becomes 1, and thus, the slope would be zero. It has been the practice (*44*) to express the limits of varying 0 to 1 in terms of the rate-constants associated with the breakdown of the central complex as in eq 9, which makes perfect physical sense.

observation of a stoichiometric burst implies $k_9 > k_{10}$, that is, the equilibrium between the central complexes involving the substrates and products favors product formation (*37*). Therefore, the rate constant of the burst phase is essentially that of the phosphoryl transfer step (k_9). From the viscosity effects and the presteady-state kinetics data, we can now deduce the values of k_6 and k_8 to be <1 s^{-1} (Table 5), which is at least10-fold less than that of k_9.

SUMMARY

Our study of the kinetic mechanism of ROCK I demonstrated that using the steady-state inhibition kinetics alone can be misleading in delineating the binding mechanism of bisubstrate reactions. The isotope partition experiment in conjunction with ATPase activity and the direct measurement of K_d values for ATP site binders presented clear evidence for the presence of a kinetically competent [E−ATP] binary complex in the ROCK I-catalyzed kinase reaction. This conclusion would have been missed if one relied entirely on inhibition kinetics. Several conclusions can be drawn about the catalytic mechanism of ROCK I from the kinetic studies. (1) The order of substrate binding is random, as with ROCK II, but the enzyme-bound species are not at rapid equilibrium with the ternary complex. The release of substrate ligands from the ternary complex (k_6 and k_8) is less favored than phosphoryl transfer (k_9). (2) The second-order rate constants for the binding of substrates (k_5 and k_7) are several orders of magnitude smaller (Table 5) than the bimolecular rate constant for diffusion. A likely scenario is that substrate binding is a two-step process, the initial collision complex formed may be rapid but weak ($K_d \sim$ mM) and is followed by a slow conformational change resulting in a lower net second-order rate constant. (3) The k_{cat} value of 1 s^{-1} for ROCK I catalysis is low compared to that of many protein kinases but is comparable to that for CSK. The active site titration of the ATPase and kinase activities using tight binding inhibitors (data not shown) confirmed that ROCK I was fully active. (4) The presence of a stoichiometric burst in the pre-steady-state kinetics suggests that k_9 is at least 10-fold larger than k_{10}, and hence, the internal equilibrium for the central complexes is favored in the direction of products. (5) The substrate and product release steps are presented with higher barriers than that for the phosphoryl transfer step.

The kinetic mechanism of PKA, a prototypic protein kinase, had been extensively investigated. As in the case of ROCK I, the chemical step is fast compared to that for the product release for PKA, and the rate-limiting step has been narrowed down to that of ADP release (*44*−*45*). Adams and co-workers, using stopped flow kinetics and fluorescently tagged PKA, have identified nucleotide-dependent conformational transitions in PKA before and after the chemical event (*46*−*49*). Because PKA and ROCK share a high degree of active site homology, it is likely that ROCK I may also experience similar nucleotide-dependent conformational changes during the kinase reaction. However, subtle differences have been observed crystallographically between the active sites (*50*) to impart selectivity for compound binding. The detailed energetics of ROCK catalysis delineated here should complement the structural studies and provide a better understanding of its action and, ultimately, lead to the development of novel therapeutics.

ACKNOWLEDGMENT

We would like to thank Paul Taslimi for bringing to our attention data concerning the fluorogenic property of staurosporine. Portions of this work were conducted within the ongoing protein kinase collaboration between Novartis Pharma AG and Vertex Pharmaceuticals.

NOTE ADDED AFTER ASAP PUBLICATION

There was an error in the *x*-axis labels in Figure 6 and the TOC in the version published ASAP June 6, 2006; the corrected version was published ASAP June 9, 2006.

REFERENCES

1. Kandabashi, T., Shimokawa, H., Mukai, Y., Matoba, T., Kunihiro, I., Morikawa, K., Ito, M., Takahashi, S., Kaibuchi, K., and Takeshita, A. (2002) Involvement of Rho-Kinase in agonist-induced contraction of arteriosclerotic human arteries, *Arterioscler., Thromb., Vasc. Biol. 22*, 243−248.
2. Watanabe, N., Kato, T., Fujita, A., Ishizaki, T., and Narumiya, S. (1999) Cooperation between mDia1 and ROCK in Rho-induced actin reorganization, *Nat. Cell. Biol. 1*, 136−143.
3. Ng, J., and Luo, L. (2004) Rho GTPase regulates axon growth through convergent and divergent signaling pathways, *Neuron 44*, 779−793.
4. Kamai, T., Tsujii, T., Arai, K., Takagi, asami, H., Ito, Y., and Oshima, H. (2003) Significant association of Rho/ROCK pathway with invasion and metastasis of bladder cancer, *Clin. Cancer Res. 9*, 2632−2641.
5. Fukata, Y., Oshiro, N., Kinoshita, N., Matsuoka, Y., Bennett, V., Matsuura, Y., and Kaibuchi, K. (1999) Phosphorylation of adducin by Rho-Kinase plays a crucial role in cell motility, *J. Cell Biol. 145*, 347−361.
6. Chevrier, V., Piel, M., Collomb, N., Saoudi, Y., Frank, R., Paintrand, M., Narumiya, S., Bornens, M., and Job, D. (2002) The Rho-associated protein kinase p160ROCK is required for centrosome positioning, *J. Cell. Biol. 157*, 807−817.
7. Seko, T., Ito, M., Kureishi, Y., Okamoto, R., Moriki, N., Onishi, K., Isaka, N., Hartshorne, D. J., and Nakano, T. (2003) Activation of RhoA and inhibition of myosin phosphatase as important components in hypertension in vascular smooth muscle, *Circ. Res. 92*, 411−418.
8. Nishikimi, t., Akimoto, K., Wang, X., Mori, Y., Tadokoro, K., Ishikawa, Y., Shimokawa, H., Ono, H., and Matsuoka, H. (2004) Fausidil, a Rho-kinase inhibitor, attenuates glomerulosclerosis in Dahl salt-sensitive rats, *J. Hypertens. 22*, 1787−1796.
9. Tramontano, A. F., O'Leary, J., Black, A. D., Muniyappa, R., Cutaia, M. V., and El-Sherif, N. (2004) Statin decreases endothelial microparticle release from human coronary artery endothelial cells: implication for the Rho-kinase pathway, *Biochem. Biophys. Res. Commun. 320*, 34−38.
10. Croft, D. R., Sahai, E., Mavria, G., Li, S., Tsai, J., Lee, W. M., Marshall, C. J., and Olson, M. F. (2004) Conditional ROCK activation in vivo induces tumor cell dissemination and angiogenesis, *Cancer Res. 64*, 8994−9001.
11. Thataux, P.-L., Bukoski, R. C., Rocha, P. N., Crowley, S. D., Ruiz, P., Nataraj, C., Howell, D. N., Kaibuchi, K., Spurney, R. F., and Coffman, T. M. (2003) Rho kinase promotes alloimmune response by regulating the proliferation and structure of T cells, *J. Immunol. 171*, 96−105.
12. Shimizu, Y., Dobashi, K., Iizuka, K., Horie, T., Suzuki, K., Tukagoshi, H., Nakazawa, T., Nakazato, Y., and Mori, M. (2001) Contribution of small GTPase Rho and its target protein ROCK in a murine model of lung fibrosis, *Am. J. Respir. Crit. Care Med. 163*, 210−217.
13. Inokuchi, K., Ito, A., Fukumoyo, Y., Matoba, T., Shiose, A., Nishida, T., Masuda, M., Morita, S., and Shimokawa, H. (2004) Usefulness of fausidil, a Rho-kinase inhibitor, to treat intractable severe coronary spasm after coronary artery bypass surgery, *J. Cardiovasc. Pharmacol. 44*, 275−277.

14. Riento, K., and Ridley, A. J. (2003) ROCKS: Multifunctional kinases in cell behavior, *Nat. Rev. Mol. Cell. Biol. 4*, 446−456.
15. Shimokawa, H. Seto, M., Katsumata, N., Amino, M., Kozai, T., Yamawaki, T., Kuwata, K., Kandabashi, T., Egashira, K., Ikegaki, I., Asano, T., Kaibuchi, K., and Takeshita, A. (1999) Rho-kinase-mediated pathway induces enhanced myosin light chain phosphorylation in a swine model of coronary artery spasm, *Cardiovasc. Res. 43*, 1029−1039.
16. Tominaga, T., Ishizaki, T., Narumiya, S., and Barber, D. L. (1998) p160ROCK mediates RhoA activation of Na-H exchange, *EMBO J. 17*, 4712−4722.
17. Sahai, E., and Marshall, C. J. (2003) Differing modes of tumor cell invasion have distinct requirements for Rho/ROCK signaling and extracellular proteolysis, *Nat. Cell Biol. 5*, 711−718.
18. Bao, W., Hu, E., Tao, L., Boyce, R., Mirabile, R., Thudium, D. T., Na, X. L., Willette, R. N., and Yue, T. L. (2004) Inhibition of Rho-kinase protects the heart against ischemia/reperfusion injury, *Cardiovasc. Res. 61*, 548−558.
19. Shiotani, S., Shimada, M., Suehiro, T., Soejima, Y., Yosizumi, T., Shimokawa, H., and Maehara, Y. (2004) Involvement of Rho-kinase in cold ischemia-reperfusion injury after liver transplantation in rats, *Transplantation 78*, 375−382.
20. Asano, M., and Nomura, Y. (2003) Comparison of inhibitory effects of Y-27632, a Rho kinase inhibitor, in strips of small and large mesenteric arteries from spontaneously hypertensive and normotensive Wistar-Kyoto rats, *Hypertens. Res. 26*, 97−106.
21. Mukai, Y., Shimokawa, H., Matoba, T., Kandabashi, T., Satoh, S., Hiroki, J., Kaibuchi, K., and Takeshita, A. (2001) Involvement of Rho-kinase in hypertensive vascular disease: a novel therapeutic target in hypertension, *FASEB J. 15*, 1062−1064.
22. Chen, X.-Q., Tan, I., Ng., H., Hall, C., Lim, L., and Leung, T. (2002) Characterization of RhoA-binding kinase ROKα implication of the pleckstrin homology domain in ROKα function using region-specific antibodies, *J. Biol. Chem. 277*, 12680−12688.
23. Doran, J. D., Liu, X., Taslimi, P., Saadat, A., and Fox, T. (2004) New insights into the structure-function relationships of Rho-associated kinase: a thermodynamic and hydrodynamic study of the dimer-to-monomer transition and its kinetic implications, *Biochem J. 384*, 255−262.
24. Trauger, J. W., Lin, F.-F, Turner, M. S., Stephens, J., and LoGrasso, P. V. (2002) Kinetic mechanism for human Rho-kinase II (ROCK II), *Biochemistry 41*, 8948−8953.
25. Amano, M., Chihara, K., Nakamura, N., Kaneko, T., Matsuura, Y., Kaibuchi, K. (1999) The COOH terminus of Rho-kinase negatively regulates rho-kinase activity, *J. Biol. Chem. 274*, 32418−32424.
26. Chen, G., Porter, M. D., Bristol, J. R., Fitzgibbon, M. J., and Pazhanisamy, S. (2000) Kinetic mechanism of the p38-α MAP Kinase: Phosphoryl transfer to synthetic peptides, *Biochemistry 39*, 2079−2087.
27. Prowse, C. N., Hagopian, J. C., Cobb, M. H., Ahn, N. G., and Lew, J. (2000) Catalytic reaction pathway for the mitogen-activated protein kinase ERK2, *Biochemistry 39*, 6258−6266.
28. Pelech, S. L., and Krebs, E. G. (1987) Mitogen-activated S6 kinase is stimulated via protein kinase C-dependent and independent pathways in Swiss 3T3 cells, *J. Biol. Chem. 262*, 11598−11606.
29. Meier, R., Alessi, D. R., Cron, P., Andjelkovic, M., and Hemmings, B. A. (1997) Mitogenic activation, phosphorylation and nuclear translocation of protein kinase B beta, *J. Biol. Chem. 272*, 30491−30497.
30. Stokoe, D., Caudwell, B., Cohen, P. T. W., and Cohen, P. (1993) The substrate specificity and structure of mitogen-activated protein (MAP) kinase-activated protein kinase-2, *Biochem. J. 296*, 843−849.
31. Kemp, B. E., Graves, D. J., Benjamini, E., and Krebs, E. G. (1977) Role of multiple basic residues in determining the substrate specificity of cyclic AMP-dependent protein kinase, *J. Biol. Chem. 252*, 4888−4894.
32. Morrison, J. F., and Stone, S. R. (1985) Approaches to the study and analysis of the inhibition of enzymes by slow- and tight-binding inhibitors, *Comments Mol. Cell. Biophys. 2*, 347−368.
33. Cha, S. (1975) Tight-binding iinhibitors-1, *Biochem. Pharmacol. 24*, 2177−2185.
34. Wilson, K. P., McCaffery, P. G., Hsiao, K., Pazhanisamy, S., Guilullo, V., Bemis, G. W., Fitzgibbon, M. J., Caron, P. R., Murco, M. A., and Su, M. S.-S. (1997) The structural basis of the specificity of p38 MAP kinase, *Chem. Biol. 5*, 423−431.
35. Rose, I. A. (1980) The isotope trapping method: desorption rates of productive E.S complexes, in *Methods in Enzymology* (Purich, D., Ed.) Vol. 64, pp 47−59. Academic press, New York.
36. Blacklow, S. C., Raines, R. T., Lim, W. A., Zamore, P. D., and Knowles, J. R. (1988) Triosephosphate isomerase catalysis is diffusion controlled. Appendix: Analysis of triose phosphate equilibria in aqueous solution by ^{31}P NMR, *Biochemistry 27*, 1158−1167.
37. Johnson, K. A. (1992) Transient-state kinetic analysis of enzyme reaction pathways, in *The Enzymes* (Sigman, D. S., Ed.) 3rd ed., pp 1−61. Academic Press, New York, .
38. Knight, W. B., and Cleland, W. W. (1989) Thiol and amino analogues as alternate substrates for glycerokinase from *Candida mycoderma*, *Biochemistry 28*, 5728−5734.
39. Schindler, J. F., Godbey, A., Hood, W. F., Bolten, S. L., Broadus, R. M., Kasten, T. P., Cassely, A. J., Hirsch, J. L., Merwood, M. A., Nagy, M. A., Fok, K. F., Saabye, M. J., Morgan, H. M., Compton, R. P., Mourey, R. J., Wittwer, A. J., and Monahan, J. B. (2002) Examination of the kinetic mechanism of mitogen-activated protein kinase activated protein kinase-2, *Biochem. Biophys. Acta 1598*, 88−97.
40. Kong, C.-T, and Cook, P. F. (1988), Isotope partitioning in the adenosine 3′,5′-monophosphate dependent protein kinase reaction indicates a steady-state random kinetic mechanism, *Biochemistry 27*, 4795−4799.
41. Whitehouse, S., Feramisco, J. R., Casnellie, J. E., Krebs, E. G., and Walsh, D. A. (1983) Studies on the kinetic mechanism of the catalytic subunit of the cAMP-dependent protein kinase, *J. Biol. Chem. 258*, 3693−3701.
42. Segel, I. H. (1975) in *Enzyme Kinetics*, pp283−291, John Wiley & Sons, New York.
43. Cleland, W. W. (1982) Use of isotope effects to elucidate enzyme mechanisms, *Crit. Rev. Biochem. 13*, 385−428.
44. Adams, J. A, and Taylor, S. S. (1992) Energetic limits of phosphotransfer in the catalytic subunit of cAMP-dependent protein kinase as measured by viscosity experiments, *Biochemistry 31*, 8516−8522.
45. Grant, B. D., and Adams, J. A. (1996) Pre-steady-state kinetic analysis of cAMP dependent protein kinase using rapid quench flow techniques, *Biochemistry 35*, 2022−2029.
46. Zhou, J., and Adams, J. A. (1997) Participation of ADP dissociation in the rate-determining steps in cAMP-dependent protein kinase, *Biochemistry 36*, 15733−15738.
47. Lew, J., Taylor, S. S., and Adams, J. A. (1997) Identification of a partially rate-determining step in the catalytic mechanism of cAMP-dependent protein kinase: A transient kinetic study using stopped-flow fluorescence spectroscopy, *Biochemistry 36*, 6717−6724.
48. Shaffer, J., and Adams, J. A. (1999) An ATP-linked structural change in protein kinase A precedes phosphoryl transfer under physiological magnesium concentrations, *Biochemistry 38*, 5572−5581.
49. Shaffer, J., and Adams, J. A. (1999) Detection of conformational changes along the kinetic pathway of protein kinase A using a catalytic trapping technique, *Biochemistry 38*, 12072−12079.
50. Jacobs, M., Hayakawa, K., Swenson, L., Bellon, S., Fleming, M., Taslimi, P., and Doran, J. (2005) The structure of dimeric ROCK I reveals the mechanism for ligand selectivity, *J. Biol. Chem. 281*, 260−268.

BI052468Q